



Hydrodynamic interactions and relative motions of two floating platforms with mooring lines in side-by-side offloading operation

B.J. Koo, M.H. Kim*

Department of Civil Engineering (Ocean Engineering Program), Texas A&M University, College Station, TX 77843, United States

Received 29 January 2005; received in revised form 18 January 2006; accepted 9 February 2006

Available online 5 June 2006

Abstract

The hydrodynamic interaction and mechanical coupling effects of two floating platforms connected by elastic lines are investigated by using a time-domain multi-hull/mooring/riser coupled dynamics analysis program. Particular attention is paid to the contribution of off-diagonal hydrodynamic interaction terms on the relative motions during side-by-side offloading operation. In this regard, the exact method (CMM: combined matrix method) including all the vessel and line dynamics, and the 12×12 hydrodynamic coefficients in a combined matrix is developed. The performance of two typical approximation methods (NHI/No Hydrodynamic Interaction: iteration method between two vessels without considering hydrodynamic interaction effects; SMM/Separated Matrix Method: iteration method between two vessels with partially considering hydrodynamic interaction effects, i.e. ignoring off-diagonal cross-coupling terms in the 12×12 hydrodynamic coefficient matrix) is also tested for the same side-by-side offloading operation in two different environmental conditions. The numerical examples show that there exists significant discrepancy at sway and roll modes between the exact and the approximation methods, which means that the cross-coupling (off-diagonal block) terms of the full hydrodynamic coefficient matrix play an important role in the case of side-by-side offloading operation. Therefore, such approximation methods should be used with care. The fender reaction forces, which exhibit large force with contact but no force without contact, are also numerically modeled in the present time-domain simulation study.

© 2006 Elsevier Ltd. All rights reserved.

Keywords: Multiple floating problems; Hydrodynamic interactions; Coupling between vessels and lines; Mooring and hawser; Existing approximation vs. exact methods; Fender reaction forces; Time-domain simulations

1. Introduction

As demands for oil and gas grow, field development with multiple floating platforms, which was considered to be very challenging in the past, is becoming more and more common nowadays. One example is the FPSO (Floating Production Storage and Offloading) operation to shuttle tankers. Another example is the combination of TLP (Tension Leg Platform), drilling barge, and floating FSU (Floating Storage Unit). Recently, the demand for clean energy, such as LNG (Liquefied Natural Gas), is rapidly growing, and near-shore or offshore floating LNG terminals have been proposed. In such a case, LNG carriers should be operated in the proximity of the terminal and the effects of hydrodynamic interactions have to be carefully taken into consideration for the safe operation.

The FPSO to shuttle tankers is much cheaper than installing new underwater pipelines in a remote deepwater oil and gas field. In such a case, the tandem offloading with floating hose is a common and safe practice. However, the offloading operation from the LNG terminal to the LNG carrier should be done with great care since the flow lines have to overcome extremely low temperature, and the arrangement and the gap distance are restricted by the arm-length of LNG off-loading lines. The most feasible and economical practice seems to be the side-by-side offloading operation using conventional LNG off-loading lines. Therefore, the study of hydrodynamic interaction effects between the two large-volume floating bodies in close proximity should be an important element of the development, operation, and downtime analysis of a floating-LNG-terminal system.

The hydrodynamic interactions between multiple bodies have been reported by many researchers; Ohkushu [23], Kodan [14] and Fang and Kim [5] analyzed the hydrodynamic

* Corresponding author. Fax: +1 9797862 8162.

E-mail address: m-kim3@tamu.edu (M.H. Kim).

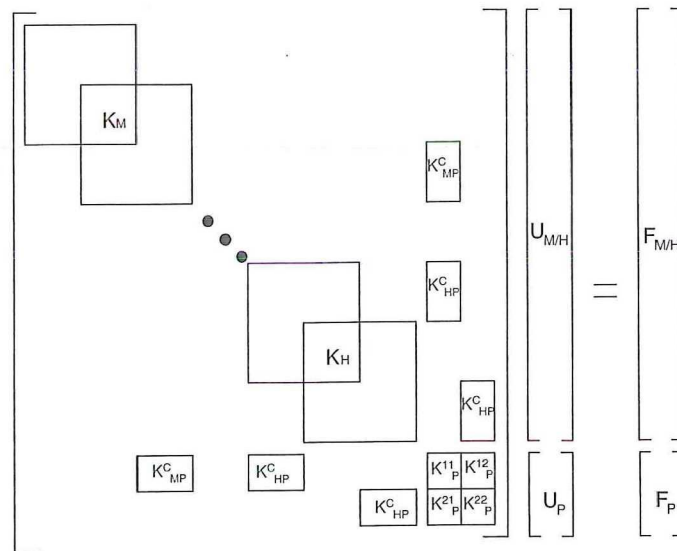


Fig. 1. Global matrix of CMM (combined matrix method) (example for two bodies).

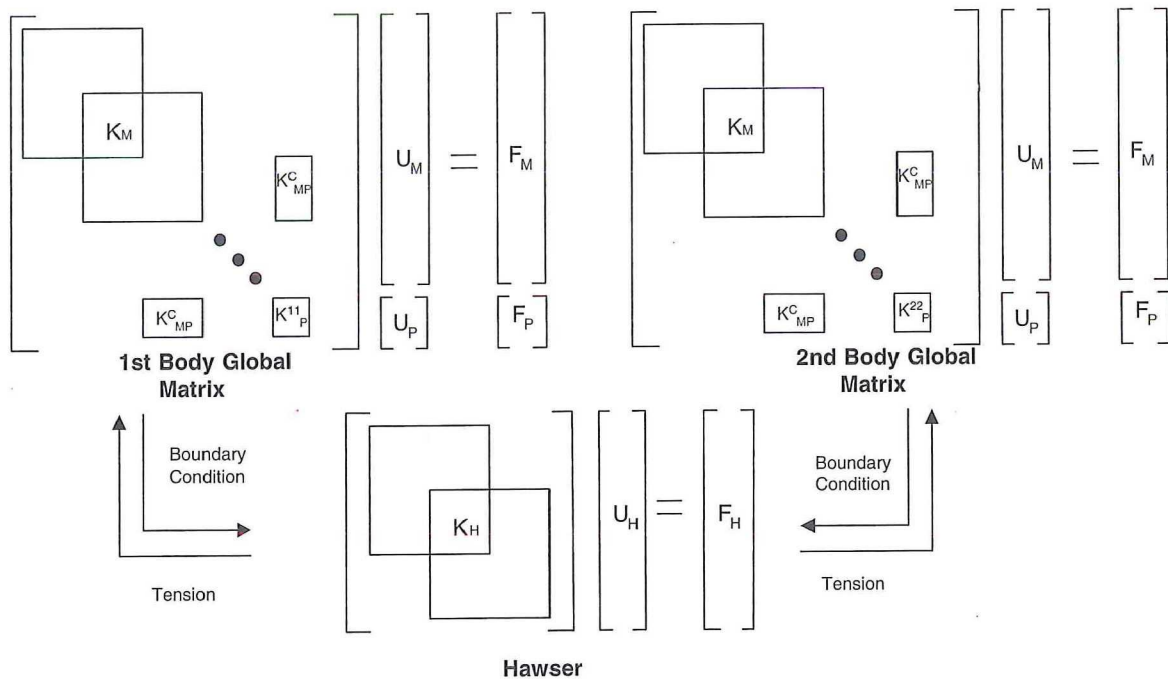


Fig. 2. Global matrix of SMM (separated matrix method) (example for two bodies).

interaction by using 2D-like strip theory. Van Oortmerssen [26] and Loken [20] used the linear diffraction theory with constant panel method, while Choi and Hong [4] employed an HOBEM (higher order boundary element method) to study three-dimensional hydrodynamic interactions between two vessels. On the other hand, multiple-body interaction in the time domain was studied by Buchner et al. [3], Hong et al. [7], Lee [17] and Kim [13]. They calculated hydrodynamic coefficients from the frequency-domain linear diffraction program, and then utilized those coefficients for ensuing time-domain simulations. Hong et al. [7] compared the potential-based computation with their experimental results for two vessels in side-by-side offloading operation with small gap. The comparison of motions and

drift forces including the free-surface elevation at the gap was reasonable. A similar comparison was also made by Kim [13].

To evaluate the responses of multiple floating platforms connected by lines more accurately, there are additional aspects to be considered. The first aspect is mechanical coupling between the multi-bodies. Second, floating platforms possess many slender members, such as mooring lines, risers, and hawsers, and their coupling effects with the hull should be carefully accounted for. In the present paper, the hull/mooring/triser/hawser dynamic coupling effects as well as hydrodynamic interactions between two vessels are fully taken into consideration. In other studies of FPSO-shuttle offloading operability, Sphaier et al. [25] and Lee and Choi [19] used a set

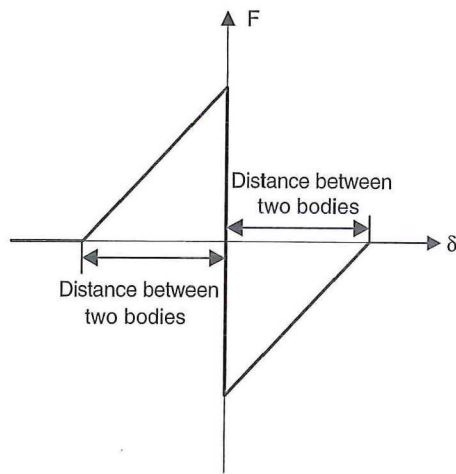


Fig. 3. Force–displacement curve for the fender.

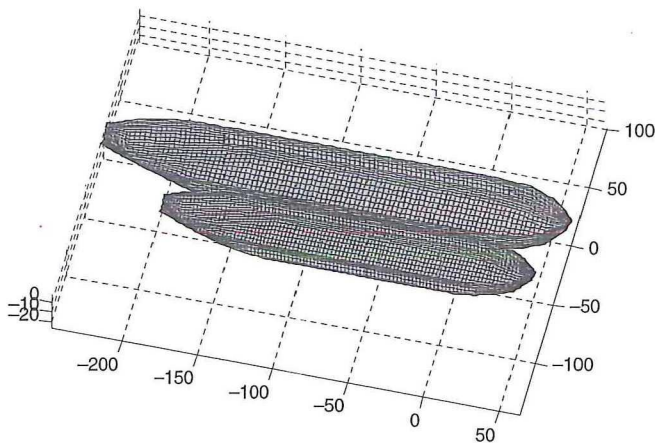


Fig. 4. Mesh generation of side-by-side moored FPSO/LNG and LNG carrier.

of simplified ship-maneuvering equations. However, this kind of much simpler approach may not be able to include all the complicated features of two-body hydrodynamic interactions.

The dynamic coupling between the hull and slender members can be evaluated in several different ways. One simple approach is called uncoupled analysis, which assumes that the mooring lines, risers, and hawsers respond statically (as a massless nonlinear spring) to hull motion (e.g. [17]). With this assumption, the inertia and damping effects as well as hydrodynamic loading on the slender members are not accounted for. When necessary, the mooring dynamics are evaluated separately as a post processing after obtaining the fairlead motions. The reliability and accuracy of this approach depend on platform-mooring types and water depth. Kim et al. [9,10] and Ma et al. [21] showed that such an uncoupled analysis of TLPs and spars may be inaccurate when used in deep water. Wichers et al. [27,28] showed that the uncoupled analysis may give even larger error in the case of FPSO or LNG/FPSO. Wichers et al. [27,28] recommended the fully-coupled dynamic models to more reliably estimate realistic design values.

In the present paper, the side-by-side offloading operation from a turret-moored FPSO to hawser-connected shuttle tankers

is investigated. The turret-moored weathervaning FPSOs are more difficult to analyze motions than spread-moored FPSOs due to the fact that they may undergo large yaw motions and wind–wave–current loads are generally sensitive to them. Therefore, to evaluate more reliably the responses of turret-moored FPSOs and shuttle tankers in wind, wave, and current, the effects of large yaw motion should be considered. Wichers [29], Kim and Kim [11] and Kim [13], for example, included such effects. Arcandra et al. [2] investigated such effects in more detail.

To verify the developed numerical simulation method, a series of large-scale experiments was conducted in the 3D OTRC wave basin at Texas A&M University for a turret-moored FPSO designed for 6000 ft water depth. The numerically simulated FPSO global motions for a non-parallel wind–wave–current environment were systematically compared with those measured from experiments. They were in good agreement, as reported in [12]. In the present study, the numerical analysis is further extended to two large vessels operating in close proximity in side-by-side offloading operation.

The time-domain hull/mooring/riser/hawser coupled dynamic analyses including two vessels were carried out by three different methods, i.e. first, based on the exact combined full-matrix method (CMM) [13]; second, an iterative separated-matrix method (SMM); and third, a no-hydrodynamic-interaction (NHI) method. Using the iterative separated matrix method, the hydrodynamic interactions are not fully captured but the corresponding module development can be greatly simplified and the resulting matrix size and computational time can be reduced by solving the individual vessels separately in an iterative manner. However, the reliability of such a simplified method has to be checked against the combined full matrix method. To the best of the authors' knowledge, this kind of comparison has not been published yet. The main objective of this study is to assess the performance of the three different approaches for side-by-side offloading operation with various environmental conditions. Finally, the effects of fender-induced contact loading are also numerically modeled and analyzed in a similar way to that of Koo et al. [15], which is possible only in the time-domain approach.

2. Formulation

2.1. Hydrodynamics of multiple floating bodies in time-domain analysis

When a large three-dimensional body interacts with incident waves, the hydrodynamic coefficients and wave exciting forces and moments can be obtained by using the first- and second-order diffraction/radiation theory. In the diffraction/radiation theory, the total velocity potential can be decomposed into incident, diffraction, and radiation potentials. The total velocity potential satisfies the Laplace equation as a governing equation and all the requisite boundary conditions along the closed boundary including bottom, free surface, body boundary, and radiation boundary. The rigid-body motion of a single floating

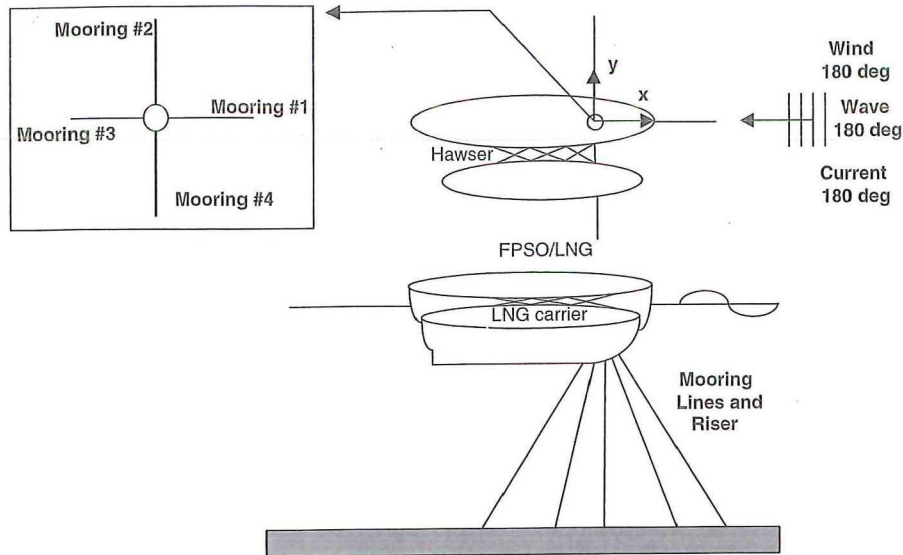


Fig. 5. Arrangement of mooring system, riser and hawser for side-by-side moored FPSO/LNG and LNG carrier.

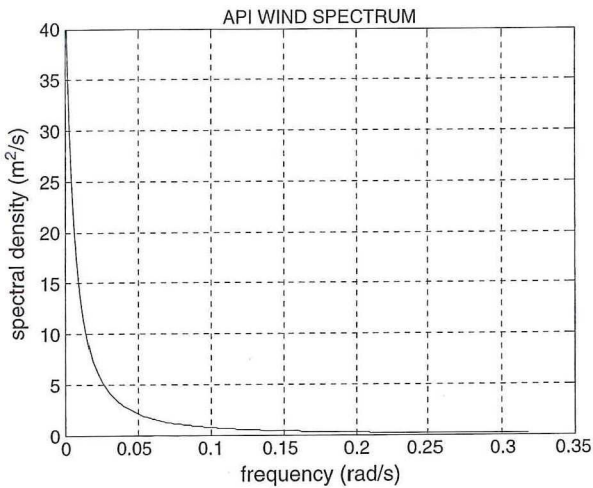


Fig. 6. API wind spectrum (at 10 m above MWL, $V_{10} = 5.0$ m/s).

body can be described by 6-DOF (degree of freedom) motions. Therefore, for N multiple floating bodies, $6N$ -DOF motions have to be simultaneously solved, i.e. one diffraction problem with all the body fixed and $6N$ radiation problems in which a motion is prescribed on one body while all the other bodies are fixed. Therefore, the interaction effects come from both the diffraction and radiation problems. In the present paper, the detailed hydrodynamic formulations for N bodies are not presented. Readers are directed to [13] for the details.

To obtain all the hydrodynamic coefficients of N bodies, such as added mass, radiation damping, first- and second-order wave-frequency and mean-drift forces, a three-dimensional second-order diffraction/radiation panel program WAMIT [18] was used. The computed frequency-domain hydrodynamic coefficients are used in the time-domain equation expressed by a two-term Volterra series expression via a Kramers–Kronig relation. In the time-domain equation, the frequency-dependent radiation damping is included in the form of a convolution integral. When computing the convolution integral of multiple

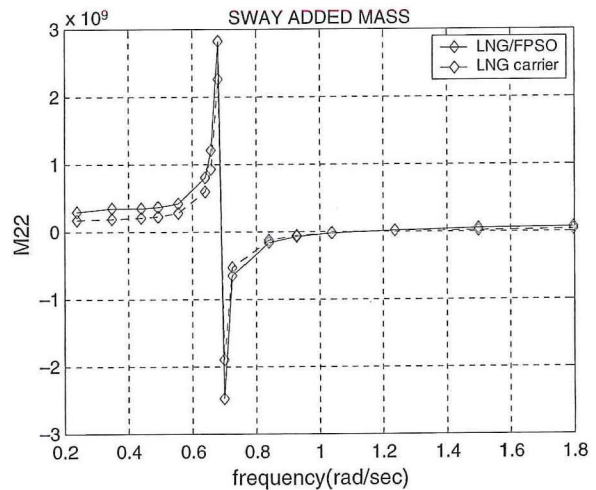
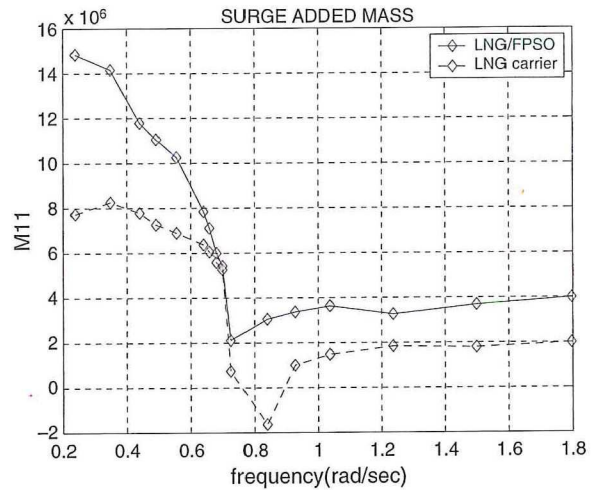


Fig. 7. Added mass of LNG/FPSO and LNG carrier for 5 m gap.

bodies, the retardation function (Fourier cosine transform of the radiation damping) can be highly oscillatory and slowly

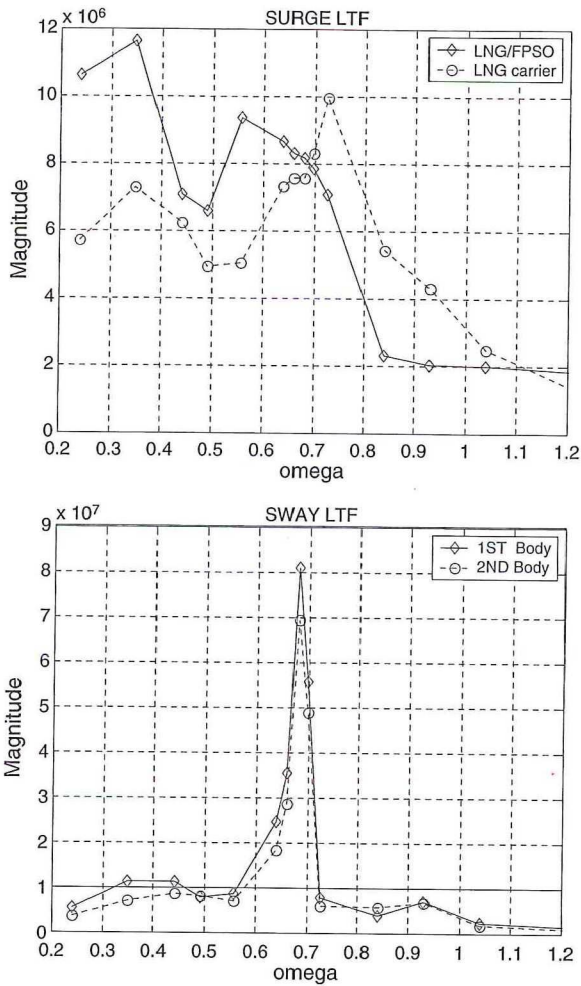


Fig. 8. Linear wave-force transfer function of LNG/FPSO and LNG carrier for 5 m gap.

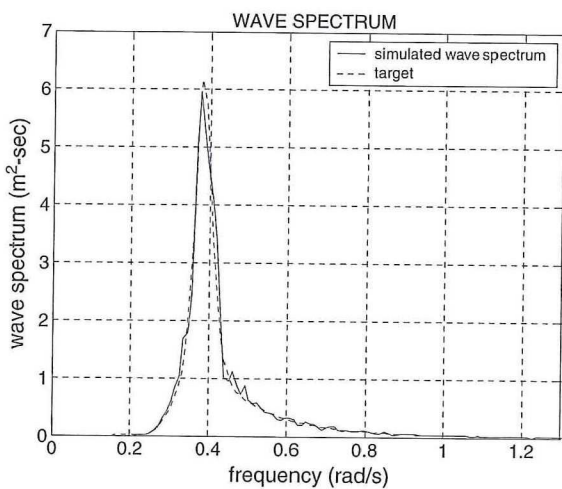


Fig. 9. Wave amplitude spectrum (side-by-side Case 1).

decay, so special attention should be paid, as pointed out by Hong et al. [7].

In the present case studies, the surge–sway–yaw natural frequencies are very small, thus only the second-order difference-frequency forces near the diagonal (mean-drift) of

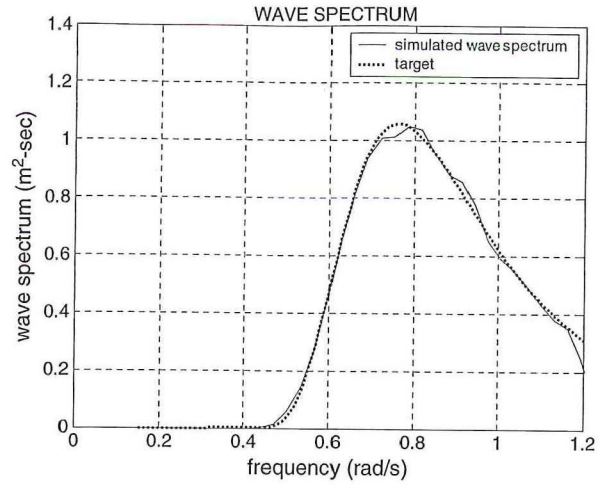


Fig. 10. Wave amplitude spectrum (side-by-side Case 2).

the QTF (Quadratic Transfer Function) are required, which justifies the use of the so-called Newman’s approximation. It is shown in [13] that this simpler approach produces reasonable results in the case of a turret-moored FPSO when compared with the more accurate, time-consuming full-QTF method. In this paper, Newman’s approximation is employed for the numerical examples. The wave drift damping was calculated by Aranha’s formula for the same turret-moored FPSO; its effects are found to be small [1], and thus wave drift damping is not considered in this study.

To calculate the responses of N floating bodies, the equation of motion can be expressed as follows:

$$\begin{bmatrix} M_1 + m_{1,1}^a(\infty) & \dots & m_{1,N}^a(\infty) \\ \vdots & \ddots & \vdots \\ m_{N,1}^a(\infty) & \dots & M_N + m_{N,N}^a(\infty) \end{bmatrix} \begin{Bmatrix} \ddot{x}_1 \\ \vdots \\ \ddot{x}_N \end{Bmatrix} + \begin{bmatrix} \int R_{11}(t-\tau)d\tau & \dots & \int R_{1,N}(t-\tau)d\tau \\ \vdots & \ddots & \vdots \\ \int R_{N,1}(t-\tau)d\tau & \dots & \int R_{N,N}(t-\tau)d\tau \end{bmatrix} \begin{Bmatrix} \dot{x}_1 \\ \vdots \\ \dot{x}_N \end{Bmatrix} + \begin{bmatrix} K_1 & \dots & \vdots \\ \vdots & \ddots & \vdots \\ \vdots & \dots & K_{N,N} \end{bmatrix} \begin{Bmatrix} x_1 \\ \vdots \\ x_N \end{Bmatrix} = \begin{Bmatrix} \vec{F}_1 \\ \vdots \\ \vec{F}_N \end{Bmatrix} \quad (1)$$

where $[M]$ is the 6×6 structure mass sub-matrix, $[m]$ is the added mass sub-matrix at infinite frequency, $[R]$ is the retardation function sub-matrix, $[K]$ is the hydrostatic restoring-coefficient sub-matrix, $[x]$ is the motion vector in the group, and $[F]$ is the external force vector in the group. The subscript represents the body number. The force vector includes the wave-frequency exciting force, wind force, current force, and slowly varying wave drift force.

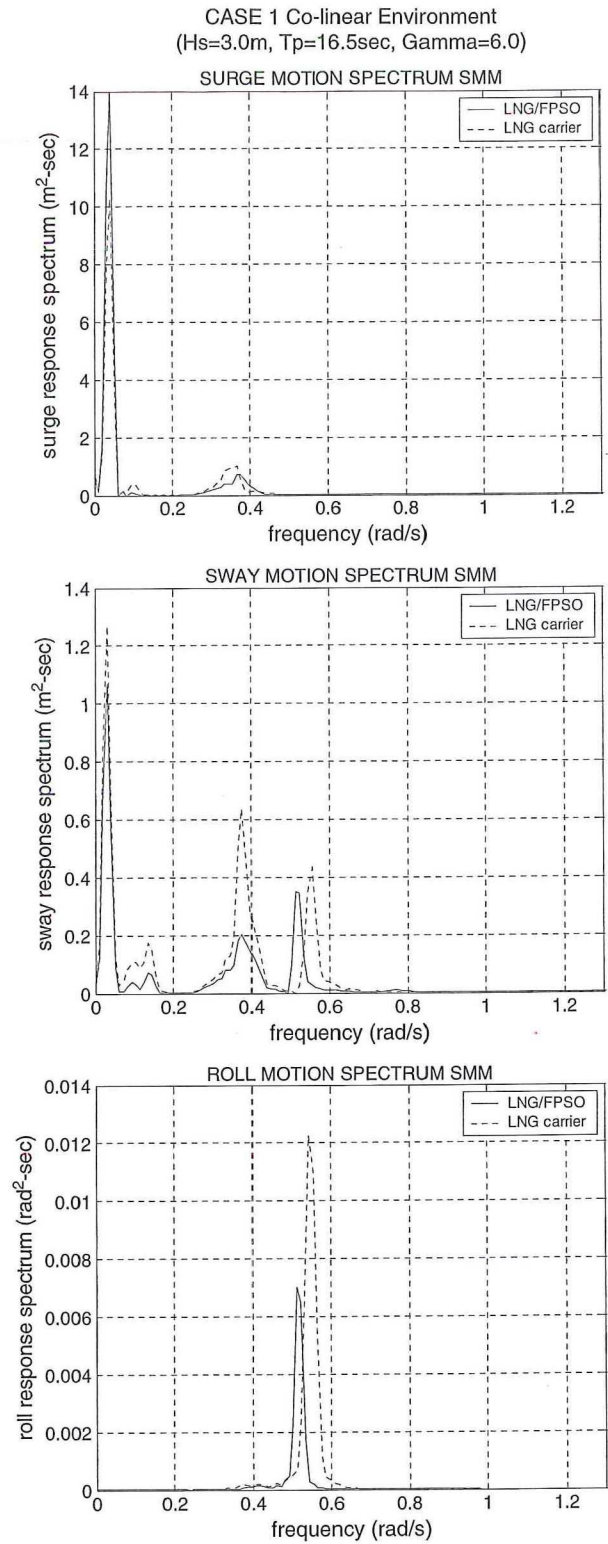
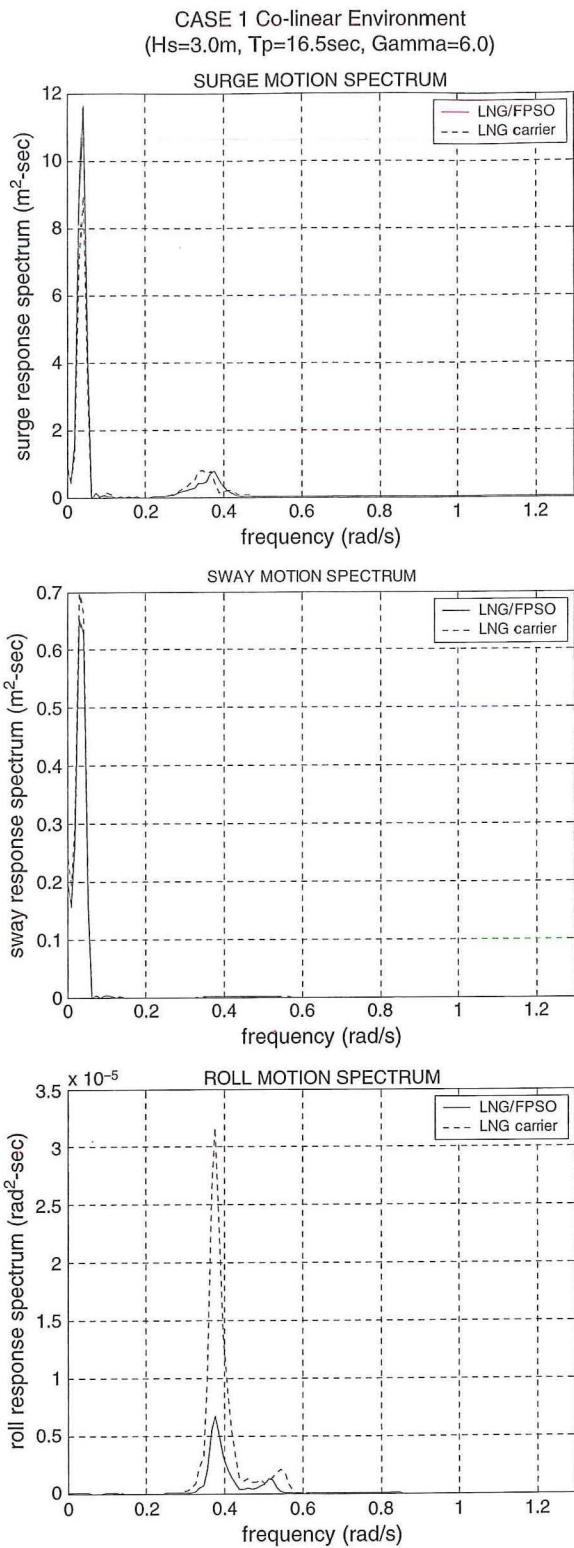


Fig. 11. Motion amplitude spectra (without hydrodynamic interaction Case 1).

Fig. 12. Motion amplitude spectra (SMM Case 1).

2.2. Mechanical coupling between multiple floating bodies and slender members

To analyze the coupled dynamics of multiple floating bodies with mooring lines, risers, and hawsers in the most accurate manner, a big combined matrix including all the

rigid bodies and slender members and their interactions should be solved simultaneously as an integrated system. For the static/dynamic analyses of slender members, an extension of the theory developed by Garrett [6] was used. The methodology for the coupled dynamics of multiple floating

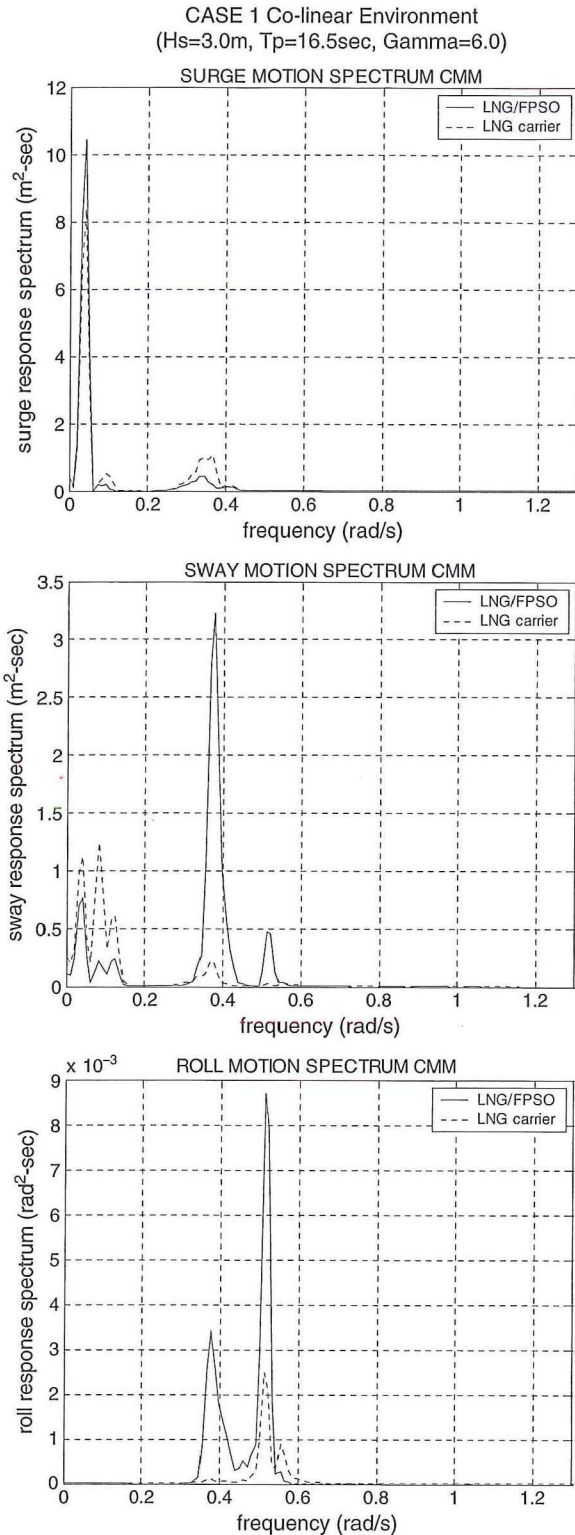


Fig. 13. Motion amplitude spectra (CMM Case 1).

platforms including slender members is in general similar to that of a single body [15], which is briefly summarized in the following.

Assuming no torque or external twisting moment, one can derive the linear momentum-conservation equation with respect to a position vector $\vec{r}(s, t)$ that is a function of arc length (s) and

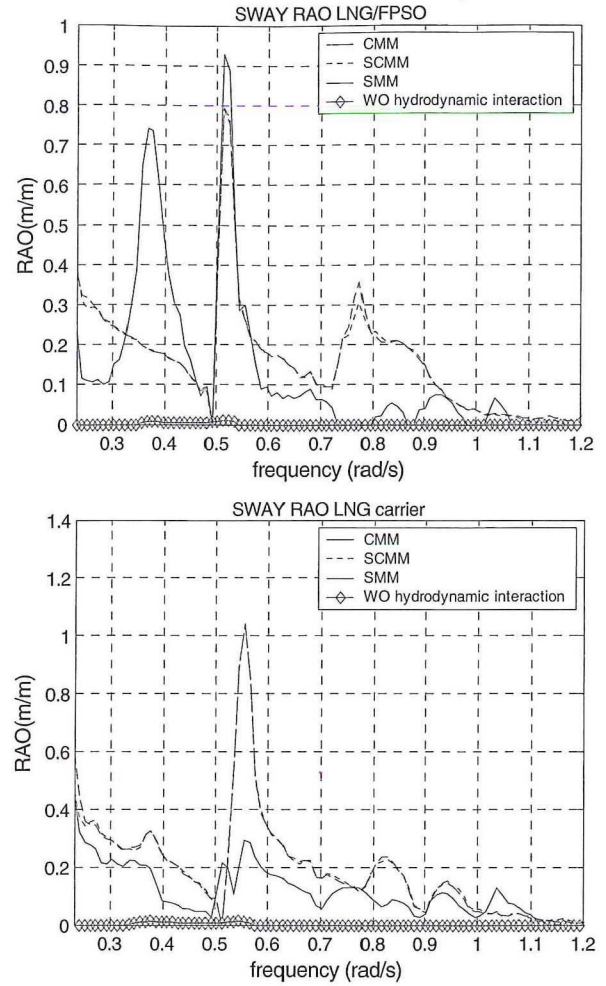


Fig. 14. Sway RAOs obtained from time-domain coupled analysis (side-by-side moored LNG/FPSO and LNG carrier for Case 1).

time (t):

$$-(B\vec{r}'')'' + (\lambda\vec{r}')' + \vec{q} = m\ddot{\vec{r}} \quad (2)$$

$$\lambda = T - B\kappa^2 \quad (3)$$

$$T = T_0 + P_e A_e - P_i A_i \quad (4)$$

where prime and dot denote spatial and time derivatives, respectively, $B = EI$ ($E =$ Young's modulus, $I =$ sectional moment of inertia) is the bending stiffness, T the local effective tension, κ the local curvature, m the mass per unit length, \vec{q} the distributed force on the rod per unit length, T_0 the local tension, P_e the external pressures, P_i the internal pressures, and A_e and A_i the external and internal cross sectional areas. The scalar variable λ can be regarded as a Lagrange multiplier.

If the rod is assumed to be inextensible, the following condition must be satisfied;

$$\vec{r}' \cdot \vec{r}' - 1 = 0. \quad (5)$$

If the rod is extensible, the condition is more generalized to

$$\frac{1}{2}(\vec{r}' \cdot \vec{r}' - 1) = \frac{T}{A_t E} \approx \frac{\lambda}{A_t E} \quad (6)$$

$$A_t = A_e - A_i. \quad (7)$$

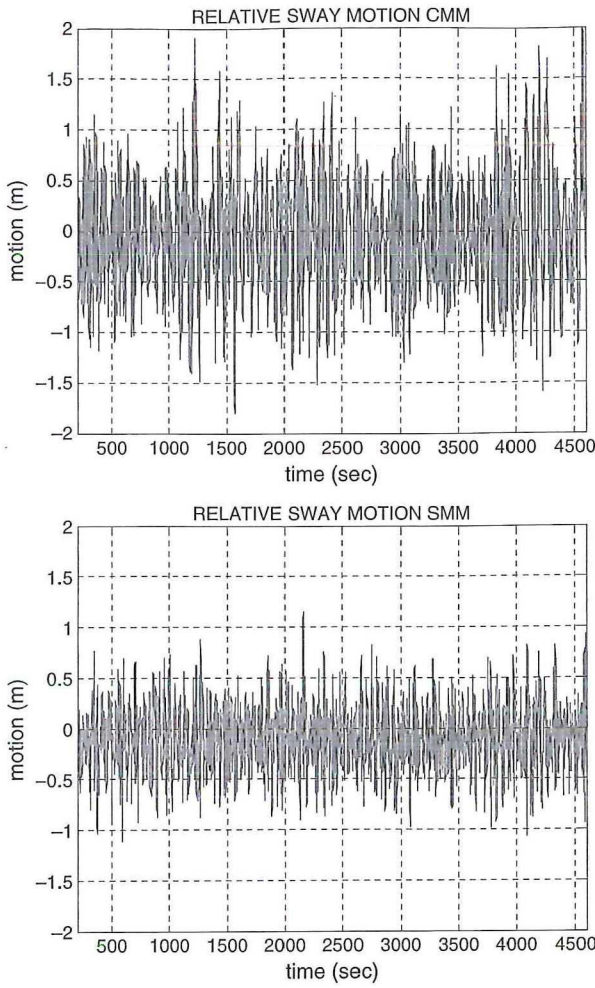


Fig. 15. Relative sway-motion time series (Case 1).

For these equations, the geometric nonlinearity is fully considered and there is no special assumption made concerning the shape or orientation of the mooring line, as long as the rod remains elastic. The benefit of this equation is that (2) is directly defined in the global coordinate system and does not require any transformations to the local coordinate system. The normal component of the distributed external force on the rod per unit length, q_n , is given by the generalized Morison equation (e.g. [24]):

$$q_n = C_I \rho A_e \dot{v}_n + \frac{1}{2} C_D \rho D |v_{nr}| v_{nr} + C_m \rho A_e \ddot{r}_n \quad (8)$$

where C_I , C_D and C_m are inertia, drag and added mass coefficients, and \dot{v}_n , v_{nr} and \ddot{r}_n are normal fluid acceleration, normal relative velocity, and normal structure acceleration, respectively. The symbols ρ and D are fluid density and local diameter. In addition, the effective weight, or net buoyancy, of the rod should be included in q_n as a static load.

To develop the finite element formulation, consider a single element of length L , and use the following expression:

$$\vec{r}(s, t) = \sum_i A_i(s) \vec{U}_i(t) \quad (9)$$

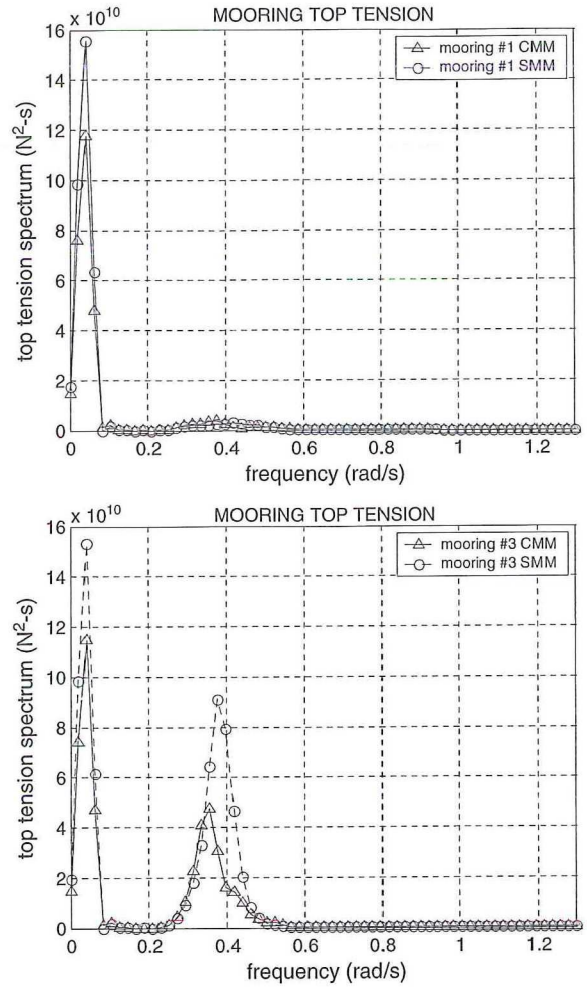


Fig. 16. Mooring top-tension spectra (Case 1).

$$\lambda(s, t) = \sum_m P_m(s) \lambda_m(t) \quad (10)$$

where A_i and P_m are interpolation functions defined on the interval $0 \leq s \leq L$. Using Eqs. (9) and (10), Eq. (2) can be reduced to the following equation by the Galerkin method and integration by parts [6]:

$$\int_0^L \left[B \vec{r}'' A_i' + \lambda \vec{r}' A_i' - \vec{q} A_i + m \ddot{\vec{r}} A_i \right] ds = B \vec{r}'' A_i' \Big|_0^L + \left\{ \lambda \vec{r}' - (B \vec{r}'')' \right\} A_i \Big|_0^L \quad (11)$$

where it is assumed that the shape function A_i is continuous on the element. The first boundary term of the right-hand side is related to the moments on the ends, and the second term is the force on the ends, i.e. they are natural boundary conditions. If Eq. (6) is used, we obtain:

$$\int_0^L P_m \left\{ \frac{1}{2} (\vec{r}' \cdot \vec{r}' - 1) - \frac{\lambda}{A_i E} \right\} ds = 0. \quad (12)$$

The position vector, its tangent, and the Lagrange multiplier are selected to be continuous at a node between adjacent elements. The interpolation functions A_i and P_m are chosen to

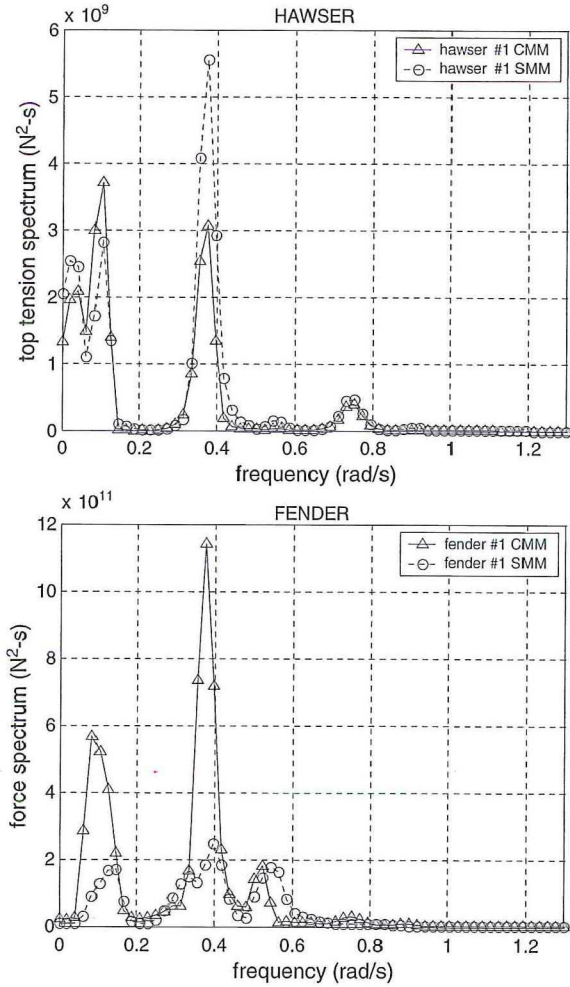


Fig. 17. Hawsers top-tension and fender-force spectra (Case 1).

be Hermitian cubic and quadratic functions of s as follows:

$$\begin{aligned} A_1 &= 1 - 3\xi^2 + 2\xi^3, & A_2 &= \xi - 2\xi^2 + \xi^3, \\ A_3 &= 3\xi^2 - 2\xi^3, & A_4 &= -\xi^2 + \xi^3 \end{aligned} \quad (13)$$

$$\begin{aligned} P_1 &= 1 - 3\xi + 2\xi^2, & P_2 &= 4\xi(1 - \xi), \\ P_2 &= \xi(2\xi - 1) \end{aligned} \quad (14)$$

where $\xi = s/L$. The parameters \vec{U} and λ are thus:

$$\begin{aligned} \vec{U}_1 &= \vec{r}(0, t), & \vec{U}_2 &= L\vec{r}'(0, t), \\ \vec{U}_3 &= \vec{r}(L, t), & \vec{U}_4 &= L\vec{r}'(L, t) \end{aligned} \quad (15)$$

$$\lambda_1 = \lambda(0, t), \quad \lambda_2 = \lambda(L/2, t), \quad \lambda_3 = \lambda(L, t). \quad (16)$$

Elements are combined using the continuity of \vec{r} , \vec{r}' and λ . The natural boundary conditions at a joint cancel out, leaving those conditions applicable at the ends of the rod. The ends of the lines are connected to the hull through a generalized elastic (both linear and rotational) spring that can also model both fixed and hinged conditions at its extreme limit. The forces and moments proportional to the relative displacements are transmitted to the hull at the connection points. The transmitted

Table I

Main particulars of the turret-moored FPSO/LNG, shuttle tanker and LNG carrier used for simulation

Designation	Unit	LNG/FPSO	LNG carrier
Length LPP	m	310.00	248.00
Breadth	m	47.17	37.74
Draft	m	18.90	15.12
Displacement	m ³	240 869.00	123 324.93
Water plane area	m ²	13 400.00	8 576.00
Center of gravity above keel	m	13.32	10.66
Transverse radius of gyration	m	15.79	12.63
Longitudinal radius of gyration	m	115.03	92.02
Yaw radius of gyration	m	116.13	92.91
Wind area frontal	m ²	1 012.00	647.68
Wind area side	m ²	3 772.00	2 414.08
Turret center line behind FPP	m	63.55	N/A

forces from the mooring lines to the platform are given by

$$\vec{F}_P = \vec{K}(\vec{T}\vec{u}_p - \vec{u}_I) + \vec{C}(\vec{T}\dot{\vec{u}}_p - \dot{\vec{u}}_I) \quad (17)$$

where \vec{K} is the stiffness matrix, \vec{C} the damping matrix, \vec{T} the transformation matrix between the platform origin and connection point, and \vec{u}_p and \vec{u}_I are displacement vectors of the platform and connection point.

The hull response equation is combined into the mooring-line equation in the time domain as follows:

$$\begin{aligned} (\vec{M} + \vec{M}_a(\infty))\ddot{\vec{u}}_p + \int_0^\infty \vec{R}(t - \tau)\dot{\vec{u}}_p d\tau + \vec{K}_H\vec{u}_p \\ = \vec{F}_D + \vec{F}^{(1)} + \vec{F}^{(2)} + \vec{F}_p + \vec{F}_{WD} \end{aligned} \quad (18)$$

where \vec{M} and \vec{M}_a are structure mass and added mass, \vec{R} the retardation function (inverse cosine Fourier transform of radiation damping), \vec{K}_H the hydrostatic restoring coefficients, \vec{F}_D the drag force matrix on the hull, $\vec{F}^{(1)}$, $\vec{F}^{(2)}$ the first- and second-order wave load matrix on the hull, \vec{F}_p the transmitted force matrix from the interface and \vec{F}_{WD} the wave drift damping force matrix. The added mass at infinite frequency is obtained from Kramers–Kronig relation. For the time series of $\vec{F}^{(1)}$, $\vec{F}^{(2)}$ and \vec{F}_{WD} , a two-term Volterra series is used. From above time-domain equation of motion, the hull/mooring line/riser coupled analysis can be achieved.

In the static analysis of mooring lines and risers, Newton's iteration method was used. Thus, the coupled force on the mooring at the $(n + 1)$ th iteration can be approximated by the rule at the (n) th iteration.

$$N_i^{(n+1)} = N_i^{(n)} + \frac{\partial N_i}{\partial r_j} \Delta r_j + \frac{\partial N_i}{\partial X_j} \Delta X_j + \frac{\partial N_i}{\partial \theta_j} \Delta \theta_j. \quad (19)$$

Similarly, the coupled force on the platform at the $(n + 1)$ th iteration can be approximated by:

$$F_i^{(n+1)} = F_i^{(n)} + \frac{\partial F_i}{\partial r_j} \Delta r_j + \frac{\partial F_i}{\partial X_j} \Delta X_j + \frac{\partial F_i}{\partial \theta_j} \Delta \theta_j \quad (20)$$

$$M_i^{(n+1)} = M_i^{(n)} + \frac{\partial M_i}{\partial r_j} \Delta r_j + \frac{\partial M_i}{\partial X_j} \Delta X_j + \frac{\partial M_i}{\partial \theta_j} \Delta \theta_j. \quad (21)$$

Table 2
Main particulars and hydrodynamic coefficients of mooring system, riser, and hawser

Designation	Unit	Mooring Line			Riser	Hawser
		Segment 1: chain	Segment 2: wire	Segment 3: chain		
Pretension	kN	1.74E+03	1.74E+03	1.74E+03	1.14E+05	8.00E+05
Length at anchor point	m	9.14E+02	1.13E+03	9.14E+02	1.81E+03	N/A
Diameter	mm	8.17E+02	6.93E+02	8.17E+02	2.76E+03	N/A
Dry weight	kg/m	5.68E+02	5.16E+01	5.68E+02	2.56E+03	2.89E+01
Wet weight	kg/m	4.94E+02	1.35E+01	4.94E+02	1.31E+03	N/A
Stiffness AE	kN	2.73E+06	5.60E+05	2.73E+06	1.69E+08	1.87E+06
Inertia normal C		2.00	1.12	2.00	1.00	N/A
Drag normal Cd		2.45	1.20	2.45	1.00	N/A

Table 3
Environmental condition for side by side moored FPSO/LNG and LNG carrier

Wave (JONSWAP)	Quantities		Wind (API)	Quantities		Current (m/s)	Quantities
		<i>Hs</i> (m)	3.0	<i>V</i> ₁₀ (m/s)	5.0		Free surface
	Direction (°)	180.0	Direction (°)	180.0		at 60.96 m	0.15
						at 91.44 m	0.50
Case 1	<i>Tp</i> (sec)	16.5					
	Gamma	6.0					
Case 2	<i>Tp</i> (sec)	8.3					
	Gamma	1.0					

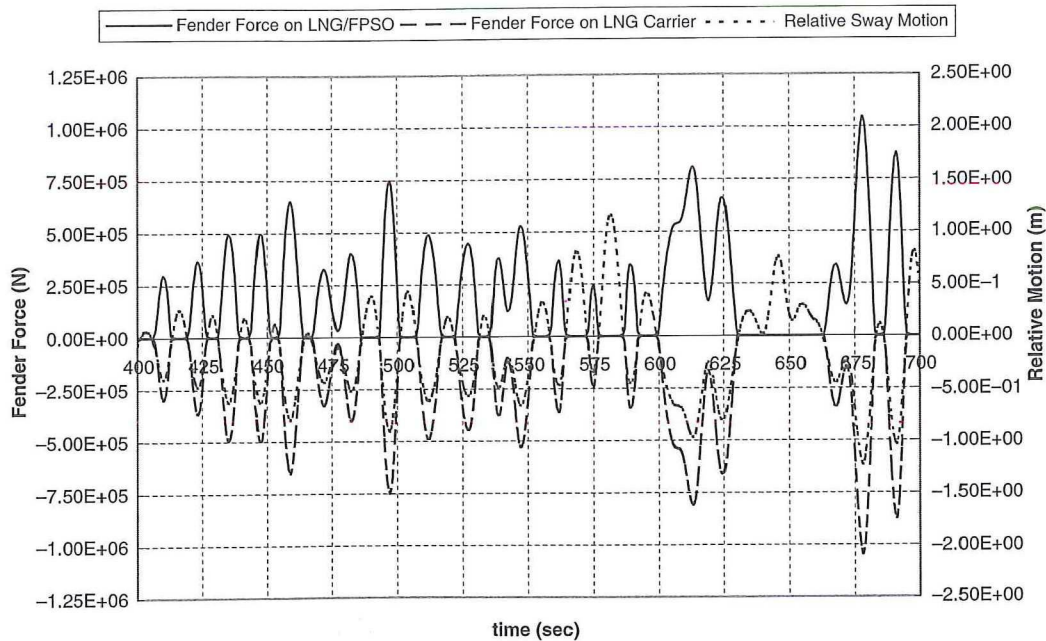


Fig. 18. Example of fender force and relative sway motion (Case 1).

Eq. (19) shows that the mooring at the connecting node is coupled with the unknown platform motion. The second terms in the right-hand side of Eqs. (19)–(21) are included in the equation of the mooring element which is coupled with the platform, while the third and fourth terms in Eqs. (19)–(21) are included in the equation of the platform. The mooring and platform are coupled by the third and fourth terms of Eq. (19) and the second term of Eqs. (20) and (21). The coupled force vectors, $N_i^{(n)}$, $F_i^{(n)}$ and $M_i^{(n)}$, are added to the force vectors at the right-hand side of the equations of the mooring element and the platform. At each iteration, the coupled

algebraic equations are solved to obtain the solutions simultaneously. The iteration continues until a specific tolerance is reached.

In the time-domain integration, the coupled force on the mooring is added to the equations of mooring and platform motions and is integrated from time $t^{(n)}$ to $t^{(n+1)}$:

$$\int_{t^{(n)}}^{t^{(n+1)}} N_i dt = \frac{\Delta t}{2} (N_i^{(n+1)} + N_i^{(n)}) \approx \frac{\Delta t}{2} \left(\frac{\partial N_i}{\partial r_j} \Delta r_j + \frac{\partial N_i}{\partial X_j} \Delta X_j + \frac{\partial N_i}{\partial \theta_j} \Delta \theta_j + 2N_i^{(n)} \right) \quad (22)$$

Table 4
Summary of motion statistics of side-by-side moored LNG/FPSO and LNG carrier (Case 1)

		Combined matrix method						Separated matrix method					
		MEAN	MIN	MAX	STD	WF	LF	MEAN	MIN	MAX	STD	WF	LF
SURGE (m)	LNG/FPSO	-4.19E-01	-2.09E+00	1.40E+00	5.39E-01	1.86E-01	5.06E-01	-4.87E-01	-2.29E+00	1.55E+00	6.20E-01	2.28E-01	5.78E-01
	LNG carrier	-1.66E-01	-1.93E+00	1.48E+00	5.45E-01	2.80E-01	4.68E-01	-1.24E-01	-1.99E+00	1.48E+00	5.76E-01	2.70E-01	5.10E-01
SWAY (m)	LNG/FPSO	2.96E-02	-1.12E+00	1.41E+00	4.13E-01	3.69E-01	1.87E-01	-5.17E-02	-9.19E-01	6.93E-01	2.40E-01	1.65E-01	1.73E-01
	LNG carrier	7.16E-02	-1.30E+00	8.77E-01	3.13E-01	1.18E-01	2.90E-01	4.82E-02	-1.03E+00	1.15E+00	3.03E-01	2.22E-01	2.06E-01
HEAVE (m)	LNG/FPSO	-5.99E-01	-1.58E+00	4.53E-01	2.57E-01	2.56E-01	4.55E-03	-6.04E-01	-1.75E+00	7.33E-01	3.46E-01	3.46E-01	1.84E-02
	LNG carrier	1.99E-03	-7.94E+00	7.92E+00	3.00E+00	3.00E+00	0.00E+00	2.19E-03	-7.41E+00	7.37E+00	2.81E+00	2.81E+00	0.00E+00
ROLL (°)	LNG/FPSO	-2.36E-03	-3.86E+00	3.55E+00	1.17E+00	1.17E+00	1.59E-02	-1.34E-03	-2.18E+00	2.23E+00	8.33E-01	8.33E-01	1.94E-02
	LNG carrier	-1.02E-02	-1.89E+00	1.96E+00	5.89E-01	5.89E-01	2.39E-02	-1.07E-02	-3.34E+00	3.22E+00	1.25E+00	1.25E+00	2.21E-02
PITCH (°)	LNG/FPSO	2.08E-01	-5.14E-01	9.33E-01	1.95E-01	1.95E-01	1.30E-03	2.09E-01	-6.13E-01	1.14E+00	2.63E-01	2.63E-01	6.30E-03
	LNG carrier	-2.25E-04	-4.21E+00	4.10E+00	1.59E+00	1.59E+00	0.00E+00	-3.26E-04	-3.88E+00	3.82E+00	1.47E+00	1.47E+00	0.00E+00
YAW (°)	LNG/FPSO	2.78E-01	-5.36E-01	9.32E-01	2.49E-01	2.05E-01	1.42E-01	4.43E-01	-1.72E-01	9.54E-01	2.24E-01	4.83E-02	2.18E-01
	LNG carrier	3.44E-01	-6.37E-01	1.09E+00	2.58E-01	1.21E-01	2.28E-01	5.24E-01	-4.14E-01	1.36E+00	2.86E-01	1.86E-01	2.18E-01

Table 5
Summary of relative-motion statistics of side-by-side moored LNG/FPSO and LNG carrier (Case 1)

	Combined matrix method				Separated matrix method		
	SURGE (m)	SWAY (m)	HEAVE (m)		SURGE (m)	SWAY (m)	HEAVE (m)
MAX	6.28E-01	1.98E+00	7.02E+00	MAX	7.04E-01	1.15E+00	6.81E+00
MIN	-1.01E+00	-1.81E+00	-8.23E+00	MIN	-1.30E+00	-1.12E+00	-8.23E+00
STD	2.55E-01	5.55E-01	2.88E+00	STD	3.25E-01	3.18E-01	2.84E+00

Table 6
Motion difference between combined matrix method and separated matrix method (Case 1)

		Difference					
		MEAN	MIN	MAX	STD	WF	LF
SURGE (m)	LNG/FPSO	6.73E-02	2.00E-01	-1.55E-01	-8.12E-02	-4.18E-02	-7.13E-02
	LNG carrier	-4.28E-02	5.92E-02	-6.23E-03	-3.11E-02	9.97E-03	-4.17E-02
SWAY (m)	LNG/FPSO	8.14E-02	-1.99E-01	7.17E-01	1.74E-01	2.03E-01	1.34E-02
	LNG carrier	2.34E-02	-2.76E-01	-2.75E-01	9.59E-03	-1.04E-01	8.35E-02
HEAVE (m)	LNG/FPSO	4.29E-03	1.70E-01	-2.79E-01	-8.96E-02	-8.92E-02	-1.39E-02
	LNG carrier	-2.04E-04	-5.28E-01	5.50E-01	1.91E-01	1.91E-01	0.00E+00
ROLL (°)	LNG/FPSO	-1.02E-03	-1.68E+00	1.32E+00	3.33E-01	3.34E-01	-3.51E-03
	LNG carrier	4.76E-04	1.44E+00	-1.26E+00	-6.61E-01	-6.62E-01	1.79E-03
PITCH (°)	LNG/FPSO	-1.50E-03	9.94E-02	-2.03E-01	-6.89E-02	-6.88E-02	-4.99E-03
	LNG carrier	1.01E-04	-3.28E-01	2.73E-01	1.16E-01	1.16E-01	0.00E+00
YAW (°)	LNG/FPSO	-1.65E-01	-3.63E-01	-2.16E-02	2.59E-02	1.57E-01	-7.66E-02
	LNG carrier	-1.79E-01	-2.22E-01	-2.73E-01	-2.78E-02	-6.45E-02	1.05E-02

Table 7
Summary of statistics of mooring and hawser top-tension, and fender force (Case 1)

	Combined matrix method				Separated matrix method			
	MEAN (N)	MIN (N)	MAX (N)	STD (N)	MEAN (N)	MIN (N)	MAX (N)	STD (N)
Mooring 1	4.27E+06	4.01E+06	4.48E+06	7.66E+04	4.28E+06	3.99E+06	4.51E+06	8.65E+04
Mooring 2	4.19E+06	3.86E+06	4.51E+06	1.12E+05	4.20E+06	4.04E+06	4.39E+06	5.15E+04
Mooring 3	4.12E+06	3.83E+06	4.45E+06	9.84E+04	4.11E+06	3.69E+06	4.48E+06	1.22E+05
Mooring 4	4.20E+06	3.90E+06	4.48E+06	9.22E+04	4.18E+06	3.89E+06	4.46E+06	7.84E+04
Hawser 1	1.61E+06	1.55E+06	1.70E+06	2.25E+04	1.60E+06	1.53E+06	1.70E+06	2.53E+04
Fender 1	3.44E+05	0.00E+00	1.83E+06	3.62E+05	3.17E+05	0.00E+00	1.21E+06	2.47E+05

$$\int_{t^{(n)}}^{t^{(n+1)}} F_i dt = \frac{\Delta t}{2} (F_i^{(n+1)} + F_i^{(n)})$$

$$\approx \frac{\Delta t}{2} \left(\frac{\partial F_i}{\partial r_j} \Delta r_j + \frac{\partial F_i}{\partial X_j} \Delta X_j + \frac{\partial F_i}{\partial \theta_j} \Delta \theta_j + 2F_i^{(n)} \right) \quad (23)$$

$$\int_{t^{(n)}}^{t^{(n+1)}} M_i dt = \frac{\Delta t}{2} (M_i^{(n+1)} + M_i^{(n)})$$

$$\approx \frac{\Delta t}{2} \left(\frac{\partial M_i}{\partial r_j} \Delta r_j + \frac{\partial M_i}{\partial X_j} \Delta X_j + \frac{\partial M_i}{\partial \theta_j} \Delta \theta_j + 2M_i^{(n)} \right) \quad (24)$$

Like the static analysis, the coefficients in the above equations go to the time-domain equations of the platform and the element of the mooring coupled with the platform.

2.3. CMM vs. SMM

The multi-body coupled analysis can be done by assembling the global matrix that includes all the hydrodynamic and mechanical coupling effects between vessels and slender

members. In this study, two different methods are used in assembling the global matrix. The first method is CMM (combined matrix method). In this method, all the hydrodynamic coefficients and mechanical coupling of the hull and slender members are included in one large matrix. This method in principle exactly accounts for all the hydrodynamic and mechanical interactions. The second method is SMM (separated matrix method). In this method, a global matrix is set up for each floating body and the mechanical coupling between the two vessels is calculated through the tension of hawser lines until convergence is achieved. The hawser lines are generally in the air and their length is short compared to mooring lines and risers, thus the inertia and damping effects from the hawsers are expected to be very small. The SMM can represent the mechanical coupling correctly but it cannot include the full hydrodynamic interactions. The major difference between the CMM and SMM occurs in the off-diagonal 6 × 6 added mass matrix and radiation damping matrix. Due to the separate global

Table 8
Summary of motion statistics of side-by-side moored LNG/FPSO and LNG carrier (Case 2)

		Combined matrix method						Separated matrix method					
		MEAN	MIN	MAX	STD	WF	LF	MEAN	MIN	MAX	STD	WF	LF
SURGE (m)	LNG/FPSO	6.43E-01	-9.41E-01	2.44E+00	5.74E-01	2.74E-02	5.73E-01	6.27E-01	-7.16E-01	2.11E+00	5.31E-01	2.87E-02	5.30E-01
	LNG carrier	-8.19E-01	-2.25E+00	8.38E-01	5.06E-01	4.15E-02	5.04E-01	-8.13E-01	-2.24E+00	7.16E-01	4.86E-01	4.52E-02	4.84E-01
SWAY (m)	LNG/FPSO	4.11E-01	-5.61E-01	1.49E+00	3.59E-01	5.65E-02	3.54E-01	4.18E-01	-6.32E-01	1.97E+00	3.46E-01	9.75E-02	3.32E-01
	LNG carrier	4.26E-01	-1.30E+00	1.73E+00	5.01E-01	6.95E-02	4.96E-01	4.09E-01	-1.41E+00	1.91E+00	4.77E-01	1.40E-01	4.55E-01
HEAVE (m)	LNG/FPSO	-9.01E-01	-1.12E+00	-6.67E-01	6.81E-02	6.81E-02	1.02E-03	-9.01E-01	-1.11E+00	-6.85E-01	6.73E-02	6.73E-02	5.97E-04
	LNG carrier	-5.30E-03	-2.18E-01	2.07E-01	5.41E-02	5.40E-02	4.19E-03	-5.27E-03	-1.86E-01	1.89E-01	5.20E-02	5.19E-02	3.53E-03
ROLL (°)	LNG/FPSO	-4.91E-02	-9.04E-01	7.41E-01	2.95E-01	2.92E-01	3.94E-02	-4.91E-02	-1.10E+00	7.99E-01	2.89E-01	2.86E-01	3.91E-02
	LNG carrier	6.43E-02	-1.58E+00	2.23E+00	4.18E-01	4.08E-01	8.80E-02	6.36E-02	-2.70E+00	3.40E+00	9.34E-01	9.30E-01	8.74E-02
PITCH (°)	LNG/FPSO	3.11E-01	2.12E-01	4.16E-01	2.91E-02	2.91E-02	4.21E-04	3.11E-01	2.14E-01	4.15E-01	2.80E-02	2.80E-02	2.94E-04
	LNG carrier	1.41E-04	-9.44E-02	9.98E-02	2.91E-02	2.91E-02	1.41E-03	9.40E-05	-1.46E-01	1.66E-01	3.57E-02	3.57E-02	1.06E-03
YAW (°)	LNG/FPSO	-2.22E+00	-3.96E+00	-4.82E-01	8.39E-01	2.96E-02	8.38E-01	-2.18E+00	-3.46E+00	-5.01E-01	5.81E-01	5.26E-02	5.79E-01
	LNG carrier	-2.15E+00	-3.97E+00	-2.89E-01	8.63E-01	4.84E-02	8.61E-01	-2.13E+00	-3.58E+00	-4.14E-01	6.21E-01	7.90E-02	6.16E-01

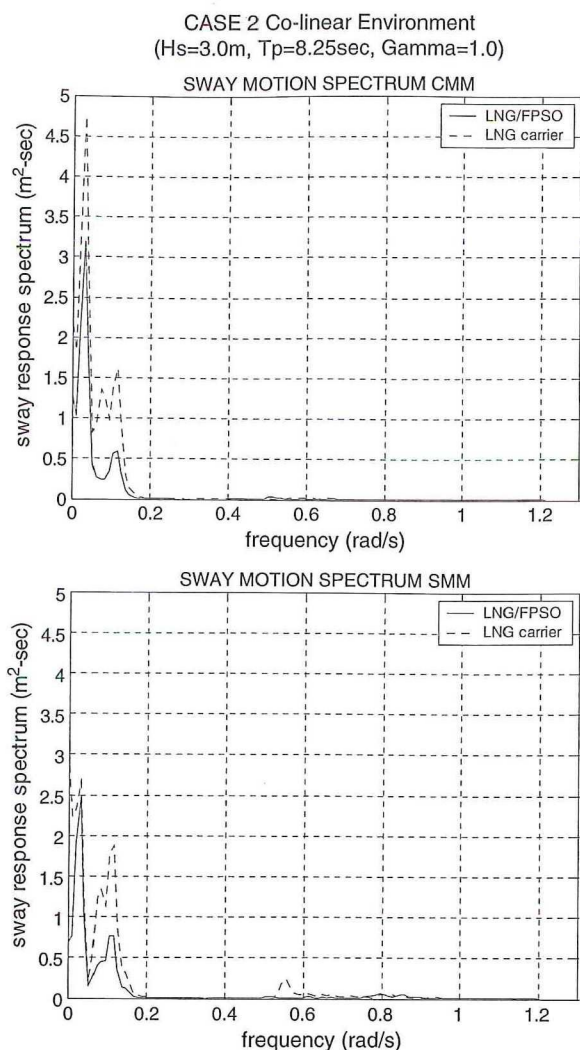


Fig. 19. Sway motion amplitude spectra (side-by-side moored LNG/FPSO and LNG carrier for Case 2).

matrix set for each body, the SMM cannot consider the off-diagonal hydrodynamic interaction terms.

The global matrix formulations are illustrated in Figs. 1 and 2, in which the sub-matrix K_M represents the coefficients for mooring lines and risers, sub-matrix K_H represents the coefficients for the hawser, sub-matrices K_{MP}^C and K_H^C represent coupling coefficients between hull and slender members, and sub-matrix K_P represents the coefficients for the hull. The superscript in the K_P matrix represents body number. The vectors U and F represent displacements and forces of the hull and slender members.

As illustrated in Fig. 1, the combined matrix method includes all the vessels and lines in one large matrix and the global matrix is inverted in every time step. Fig. 2 shows that the separated matrix method sets up the global matrix for each body and their mechanical interactions through the hawsers are solved by iteration. At each time step and iteration, the body positions are given as essential boundary conditions of the hawser end points, while the hawser tension is given to each body as external forces. Due to the separation of the global matrix, the off-diagonal (6×6) hydrodynamic

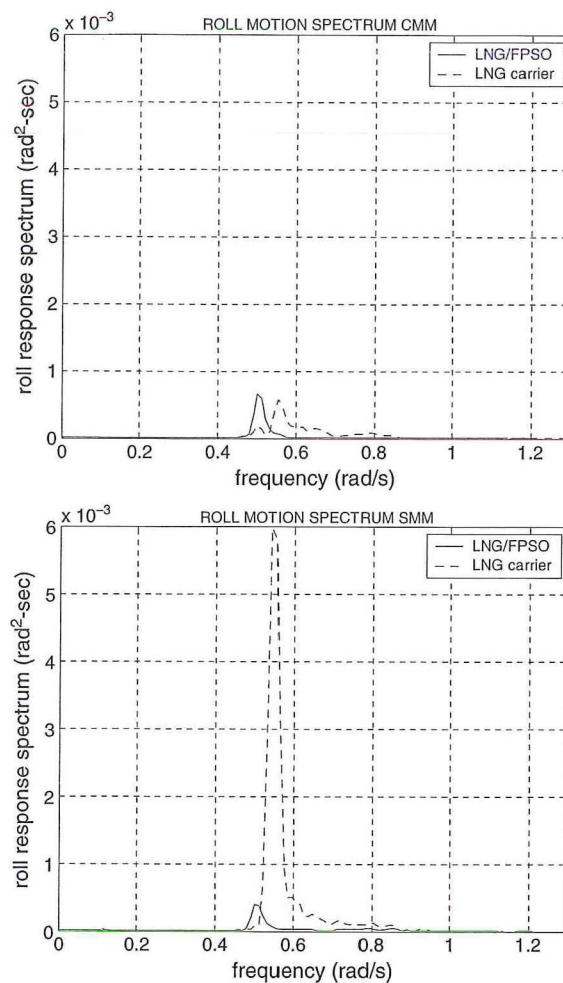


Fig. 20. Roll motion amplitude spectra (side-by-side moored LNG/FPSO and LNG carrier for Case 2).

interaction coefficients cannot be included in each separated matrix (i.e. K_P^{12} and K_P^{21} in Fig. 1). Thus, the combined matrix method is the most accurate way to calculate the multiple-floating-body interactions. However, the matrix size of the CMM increases in proportion to the number of vessels and slender members, which results in much longer computational time. Furthermore, when more than three floating bodies are involved, it is much more straightforward to use the SMM in the module development of the computer program. Under this circumstance, an important question is “how good is the SMM?” The importance of the off-diagonal (6×6) hydrodynamic interaction coefficients varies with the arrangement and distance of the two vessels. It also depends on system characteristics and environmental conditions. When hydrodynamic interaction effects are expected to be smaller than mechanical coupling effects (e.g. tandem arrangement), the SMM can be an efficient way to solve the multi-body problem [16].

2.4. Fender effects in time-domain simulation

In general, there are fenders between the LNG FPSO/terminal and the LNG carrier in a side-by-side offloading arrangement.

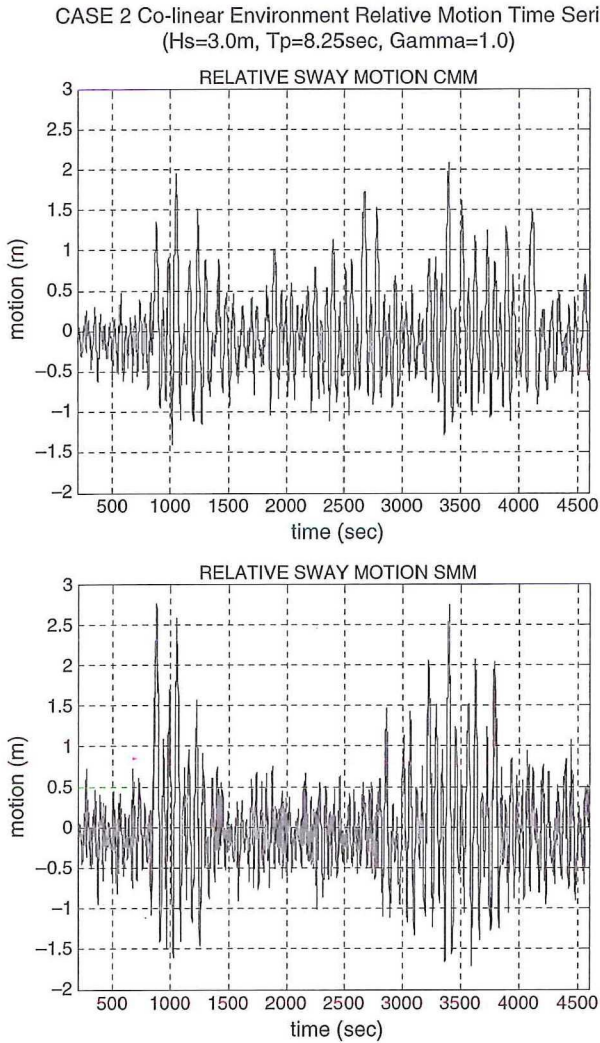


Fig. 21. Relative sway motion time series (side-by-side moored LNG/FPSO and LNG carrier for Case 2).

The function of the fender is to prevent collision between the two floating vessels. When the relative distance between the LNG terminal and the carrier is smaller than the fender length (in the present study, the initial gap), the fender exerts reaction forces on both bodies. Whereas, when the relative distance is greater than the fender length, there exist no reaction forces on both bodies. Therefore, a proper tender-reaction-force modeling is only possible in the time-domain analysis. In the present numerical simulation, the fenders are modeled as piecewise-linear gap springs for simplicity. Fig. 3 shows the force–displacement curve for the fender. Note that the fender produces equal and opposite reaction forces on both bodies only when it is compressed.

The effects of the fender can be expressed as follows:

when

$$\left| \left(X_2^1 + P_2^1 + \theta_1^1 P_3^1 - \theta_3^1 P_2^1 \right) - \left(X_2^2 + P_2^2 + \theta_1^2 P_3^2 - \theta_3^2 P_1^2 \right) \right| \geq \Delta_2 \quad \text{then} \\ N_2 = 0; \tag{25}$$

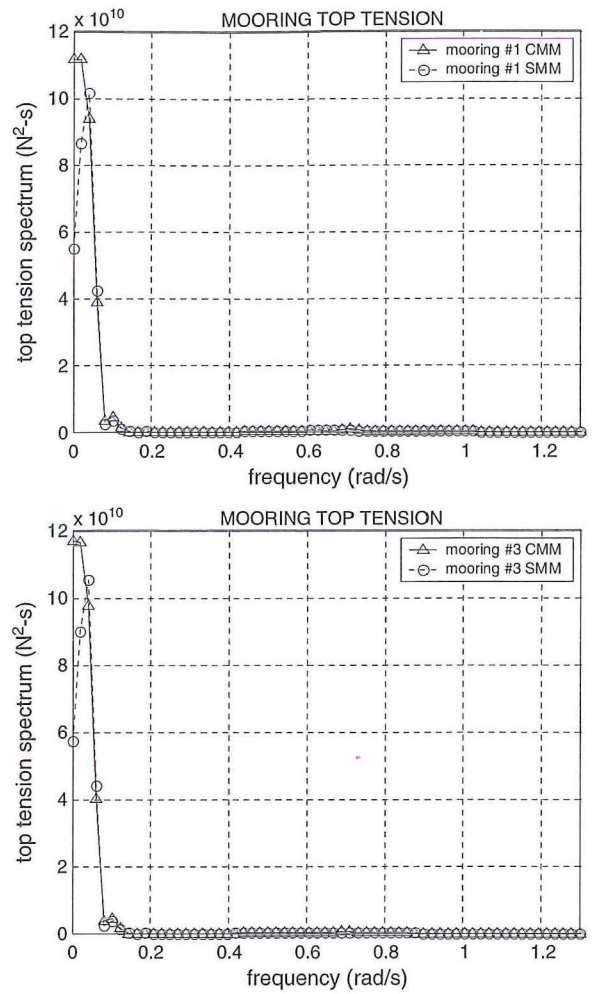


Fig. 22. Mooring top-tension spectra (Case 2).

when

$$\left| \left(X_2^1 + P_2^1 + \theta_1^1 P_3^1 - \theta_3^1 P_2^1 \right) - \left(X_2^2 + P_2^2 + \theta_1^2 P_3^2 - \theta_3^2 P_1^2 \right) \right| < \Delta_2$$

and

$$\left(X_2^1 + P_2^1 + \theta_1^1 P_3^1 - \theta_3^1 P_2^1 \right) - \left(X_2^2 + P_2^2 + \theta_1^2 P_3^2 - \theta_3^2 P_1^2 \right) < 0 \quad \text{then}$$

$$N_2 = K \left\{ \left[\left(X_2^1 + P_2^1 + \theta_1^1 P_3^1 - \theta_3^1 P_2^1 \right) - \left(X_2^2 + P_2^2 + \theta_1^2 P_3^2 - \theta_3^2 P_1^2 \right) \right] + \Delta_2 \right\}; \tag{26}$$

and when

$$\left(X_2^1 + P_2^1 + \theta_1^1 P_3^1 - \theta_3^1 P_2^1 \right) - \left(X_2^2 + P_2^2 + \theta_1^2 P_3^2 - \theta_3^2 P_1^2 \right) > 0 \quad \text{then}$$

$$N_2 = K \left\{ \left[\left(X_2^1 + P_2^1 + \theta_1^1 P_3^1 - \theta_3^1 P_2^1 \right) - \left(X_2^2 + P_2^2 + \theta_1^2 P_3^2 - \theta_3^2 P_1^2 \right) \right] - \Delta_2 \right\}; \tag{27}$$

where N is the reaction force from the fender, K is the spring constant, X is the translational motion of the rigid body, P is the position vector of the location of fender with respect to the

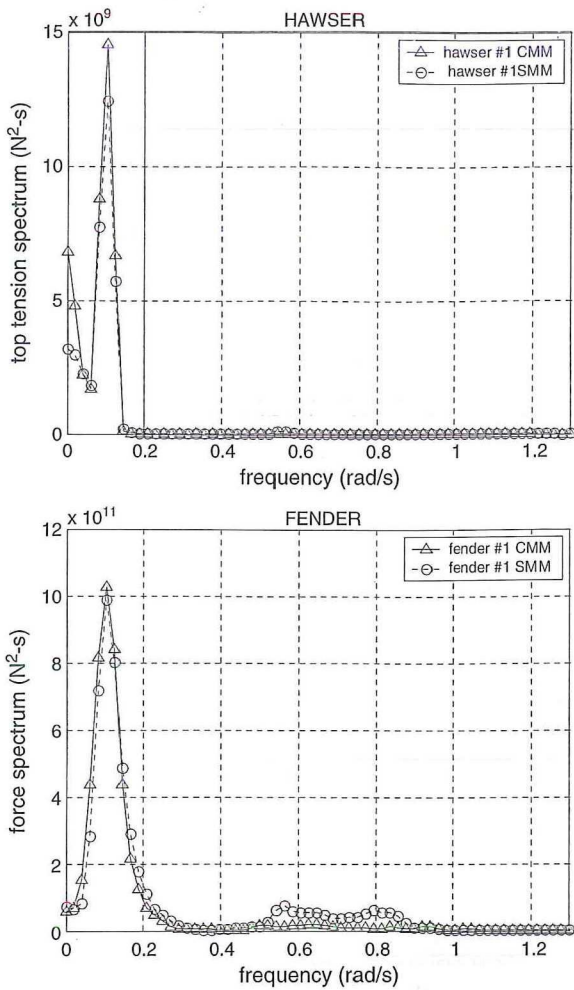


Fig. 23. Hawser top-tension and fender-force spectra (Case 2).

local coordinate of the rigid body, θ is the angular motions of the rigid body, and Δ is the initial gap between the two floating bodies. The subscript represents the direction of rigid-body motions and the superscript represents rigid-body number.

The fender forces and moments on the first body and the second body can be expressed as follows:

$$\vec{F}^1 = -\vec{N} \tag{28}$$

$$\vec{F}^2 = \vec{N} \tag{29}$$

$$\vec{M}^1 = \vec{P} \times -\vec{N} \tag{30}$$

$$\vec{M}^2 = \vec{P} \times \vec{N} \tag{31}$$

where \vec{F} is the external force on the rigid body, \vec{N} is the force from the fender, and \vec{M} is the external moment on the rigid body. The fender force is calculated from the relative displacement between the two floating bodies.

3. Numerical results and discussions: Case studies

The specifications of the LNG/FPSO and the LNG carrier used in the present study are summarized in Table 1. The LNG/FPSO originally has 12 chain–polyester–chain mooring

lines and 13 steel catenary risers. There are four groups of mooring lines; each group consists of three lines 5° apart. Each mooring line has a studless chain at both ends. The effects of tangential drag on mooring lines and Coulomb friction from the seabed were expected to be unimportant, and thus not included in this study. For simplicity, four equivalent mooring lines and one equivalent riser were used in the present simulations, with each equivalent line representing the combined effects of three mooring lines. The equivalent diameter was derived from the condition of ‘equal drag force’. Table 2 shows the main particulars and hydrodynamic coefficients of the mooring lines, risers, and hawsers. The water depth is 6000 ft (1828 m).

Numerical simulations are conducted for the case of side-by-side offloading operation with 5 m gap for two different environmental conditions. Only the collinear wind–wave–current environmental conditions from the head direction are studied here. Fig. 4 shows the distribution of panels on the LNG/FPSO and LNG carrier. Fig. 5 illustrates the mooring system, hawser connection, and environmental directions. The hawser connection is simplified compared to a more realistic and complicated one. The two environmental conditions are tabulated in Table 3. Fig. 6 illustrates the API wind spectrum used in the present simulation. As for the current and wind loading on the two vessels, the standardized OCIMF data sets [22] are used.

The second-order slowly-varying wave forces are calculated from the so-called Newman’s approximation. In other words, the off-diagonal components of the difference-frequency wave-force QTF (quadratic transfer function) are approximated by the diagonal (mean-drift) values. This approximation is valid when the natural frequencies of slowly-varying motions are small, as in the present case. Newman’s approximation may not be very reliable in the case of shallow water. The wave drift damping is expected to be small compared to other drag components, and thus is not included here [1]. The same hull damping as in [12] is used.

3.1. Side-by-side moored LNG/FPSO and LNG carrier

As mentioned earlier, the hydrodynamic interactions between two side-by-side-moored vessels have been studied by several researchers (e.g. [8,3,13] and [7]). Their results show that the sway motions of the two vessels are much larger than the single-body case in head sea conditions. To better understand the characteristics of the hydrodynamic interaction between two vessels, the hydrodynamic coefficients for a 5 m gap are presented in Figs. 7 and 8. Each figure shows the hydrodynamic coefficients of the LNG/FPSO and LNG carrier for comparison. It is interesting to notice that, near a particular frequency (i.e. 0.7 rad/s), the computed added mass and wave exciting force exhibit sharp variation. This can be explained by the pumping-mode resonance of a water column between the two bodies. Near the Helmholtz pumping resonance, the added mass can be negative. In the head sea condition, the sway-force and roll-moment of a single body should vanish due to symmetry. However, in the two-body case, their magnitudes are appreciable as a result of hydrodynamic interactions.

To evaluate the hydrodynamic interaction effects on the LNG/FPSO and LNG carrier, two environmental conditions are

Table 9
Summary of relative motion statistics of side-by-side moored LNG/FPSO and LNG carrier (Case 2)

	Combined matrix method				Separated matrix method		
	SURGE (m)	SWAY (m)	HEAVE (m)		SURGE (m)	SWAY (m)	HEAVE (m)
MAX	2.91E+00	2.09E+00	-2.44E-01	MAX	2.74E+00	2.75E+00	-3.00E-01
MIN	-1.15E-01	-1.41E+00	-9.41E-01	MIN	2.93E-01	-1.71E+00	-8.75E-01
STD	6.49E-01	5.38E-01	9.57E-02	STD	4.99E-01	6.02E-01	7.84E-02

Table 10
Motion difference between combined matrix method and separated matrix method (Case 2)

		Difference					
		MEAN	MIN	MAX	STD	WF	LF
SURGE (m)	LNG/FPSO	1.62E-02	-2.25E-01	3.29E-01	4.28E-02	-1.32E-03	4.29E-02
	LNG carrier	-5.55E-03	-1.44E-02	1.22E-01	1.93E-02	-3.67E-03	1.97E-02
SWAY (m)	LNG/FPSO	-6.52E-03	7.15E-02	-4.84E-01	1.26E-02	-4.11E-02	2.22E-02
	LNG carrier	1.72E-02	1.08E-01	-1.76E-01	2.41E-02	-7.10E-02	4.05E-02
HEAVE (m)	LNG/FPSO	-1.91E-05	-2.55E-03	1.73E-02	7.92E-04	7.86E-04	4.27E-04
	LNG carrier	-2.93E-05	-3.16E-02	1.79E-02	2.07E-03	2.03E-03	6.53E-04
ROLL (°)	LNG/FPSO	-5.60E-06	1.94E-01	-5.77E-02	6.12E-03	6.15E-03	2.70E-04
	LNG carrier	6.87E-04	1.12E+00	-1.17E+00	-5.16E-01	-5.22E-01	6.13E-04
PITCH (°)	LNG/FPSO	-5.04E-06	-1.86E-03	1.18E-03	1.10E-03	1.10E-03	1.28E-04
	LNG carrier	4.69E-05	5.18E-02	-6.60E-02	-6.57E-03	-6.59E-03	3.50E-04
YAW (°)	LNG/FPSO	-4.45E-02	-4.94E-01	1.91E-02	2.58E-01	-2.30E-02	2.59E-01
	LNG carrier	-2.10E-02	-3.89E-01	1.25E-01	2.42E-01	-3.06E-02	2.46E-01

Table 11
Summary of statistics of mooring and hawser top-tension, and fender force (Case 2)

	Combined matrix method				Separated matrix method			
	MEAN (N)	MIN (N)	MAX (N)	STD (N)	MEAN (N)	MIN (N)	MAX (N)	STD (N)
Mooring 1	4.08E+06	3.83E+06	4.31E+06	8.11E+04	4.08E+06	3.87E+06	4.28E+06	7.52E+04
Mooring 2	4.10E+06	3.93E+06	4.25E+06	5.17E+04	4.10E+06	3.90E+06	4.25E+06	4.83E+04
Mooring 3	4.23E+06	3.99E+06	4.48E+06	8.25E+04	4.22E+06	4.03E+06	4.45E+06	7.62E+04
Mooring 4	4.21E+06	4.06E+06	4.38E+06	5.19E+04	4.21E+06	4.05E+06	4.43E+06	4.92E+04
Hawser 1	1.63E+06	1.55E+06	1.72E+06	2.99E+04	1.63E+06	1.55E+06	1.72E+06	2.73E+04
Fender 1	3.26E+05	0.00E+00	1.47E+06	3.11E+05	3.22E+05	0.00E+00	1.74E+06	3.30E+05

considered. The respective wave amplitude spectra are shown in Figs. 9 and 10. To assess the acceptability of the different levels of approximation methods common in the offshore industry, three different approaches are compared.

- (1) No Hydrodynamic Interaction: hydrodynamic coefficients of respective single bodies are used.
- (2) SMM: Iterative method using separated matrices ignoring the off-diagonal 6×6 blocks in the 12×12 hydrodynamic-coefficient matrix.
- (3) CMM: Combined (whole) matrix method including all the 12×12 hydrodynamic-coefficient matrix.

The simulation results for Case 1 environmental conditions are shown in Figs. 11–13 and Tables 4–6. The most conspicuous discrepancy among the three different methods occurs in sway and roll. If the two-body hydrodynamic interaction effects are not included at all (Fig. 11), the sway and roll motions are significantly underestimated. The LNG/FPSO sway motion by

the CMM (Fig. 13), which includes all the interaction effects, is larger than that of the SMM (Fig. 12). This means that the off-diagonal blocks in the 12×12 hydrodynamic-coefficient matrix play an important role and this should not be neglected in the present case. To confirm this statement, an additional simulation is conducted by the CMM with zero off-diagonal 6×6 hydrodynamic interaction coefficients. The result (called SCMM) turns out to be the same as that of the SMM, as expected. This test also independently verifies the correctness of the SMM coding.

As can be seen in Table 4, the SMM under-predicts the LNG-FPSO sway rms by 42% (wave-frequency component by 55% and low-frequency component by 7%). On the other hand, the SMM over-predicts the LNG-carrier roll rms by 112%. The discrepancy of the shapes of the sway spectra of LNG-FPSO among the three methods is also noticeable. In CMM, wave frequency components are greater than low-frequency components. The opposite trend holds true in SMM and

No-Hydro-Interaction cases. In Fig. 11, wave-frequency sway and roll responses are very small neglecting the hydrodynamic interaction effects, as can also be seen in Fig. 14.

To see the discrepancies more clearly among the three different approaches, sway RAOs are obtained in Fig. 14 from the square-root of the ratio of the response spectrum to the wave spectrum. It has already been mentioned that the SMM and SCMM are not differentiable. For the LNG/FPSO sway RAOs, the SMM (dashed line) significantly underestimates the actual motion of CMM (solid line), especially near 0.38 rad/s. On the other hand, the SMM overestimates the actual LNG/FPSO sway motion over the range 0.6–0.9 rad/s (including Helmholtz resonance frequency). As for LNG-carrier sway motion, the SMM significantly over-predicts near 0.56 rad/s.

Fig. 15 shows the time histories of relative sway motions between the two vessels. Compared to the more accurate CMM solution, the SMM under-predicts the relative sway rms by 43% (see Table 5). Fig. 16 show the mooring-line top-tension spectra of Case 1 calculated by the CMM and the SMM. The SMM tends to over-predict the top-tension on taut line 1 and slack line 3. The taut-side mooring tension is basically quasi-static and mainly depends on slowly-varying surge motions. The surge motion spectra clearly show that the SMM overestimates both the wave-frequency and low-frequency LNG/FPSO surge motions. In the slack mooring line, the dynamic effects by wave-frequency motions are significant.

Fig. 17 show the spectra of hawser #1 top-tension and fender #1 force. The fender-force spectra clearly show the trend of under-prediction (rms by 32%) by the SMM due to smaller relative sway motions (Fig. 15). On the other hand, the wave-frequency hawser top-tension is overestimated (rms by 12%) by the SMM. The reason is that the fender forces are modeled to act against only the relative sway motion but the hawsers are influenced by both surge and sway relative motions due to its cross (X) arrangement (see Fig. 5).

Fig. 18 shows the fender-force time series. When the relative sway motion is smaller than the initial gap 5 m (negative), the fender pushes the LNG/FPSO and the LNG carrier to the opposite direction. On the other hand, when the relative sway is greater than the initial gap (positive), no force is acting on the fenders of LNG/FPSO and LNG carrier. In the present analysis, the possible Coulomb friction between the fenders of two vessels in the surge direction is not considered. Since the fender reaction force is idealized as two springs, the resulting reaction force is not impact-like but rather gradual. The more realistic impact-like results can be obtained by using quadratic or cubic force–displacement curves, as pointed out in [15]. Table 7 summarizes the mooring and hawser top-tension and fender force acting on the LNG/FPSO.

Figs. 19–23 (and Tables 8–10) show the simulation results with 8.25 s (0.76 rad/s) wave peak period (Case 2). The Case 2 wave spectrum, representing more fully-developed seas, is more wide-banded compared to Case 1. The sway results show that the SMM gives higher maximum values (32% for FPSO and 10% for carrier) compared to the CMM. The LNG-carrier roll-motion standard deviation from the SMM is twice as big as that of the CMM (see Table 8). As a result, its maximum

is over-predicted by 52%. Fig. 21 shows the time histories of the relative sway motions. The relative sway standard deviation and maximum are 12% and 32% over-predicted by the SMM. In Figs. 22 and 23, and Table 11, the spectra and statistics of the mooring top-tension, hawser tension, and fender force are given. The mooring and hawser tension are slightly under-predicted but the fender force is slightly over-predicted by the SMM.

4. Summary and conclusion

The safety and operability of side-by-side offloading operation is greatly influenced by the relative motions between adjacent vessels. Therefore, the accurate motion prediction of two vessels including all the hydrodynamic interactions with elastic lines is of great importance. The fender reaction force, which exhibits large force with contact but no force without contact, also plays a role in relative sway and yaw motions. This kind of fender-contact force can only be realized in time-domain simulations. The time-domain simulation of two vessels including all the hydrodynamic interactions, fender effects, and also the exact coupling effects with mooring lines, hawsers, and risers has never been published. This paper presents such an original study for an LNG/FPSO and an LNG-carrier in side-by-side arrangement.

Nowadays, the offshore industry analyzes the relative motions between two vessels connected by lines by two typical approximation methods: (i) NHI: an iteration method between two vessels without considering hydrodynamic interaction effects; and (ii) SMM: an iteration method between two vessels partially considering hydrodynamic interaction effects (ignoring the off-diagonal cross-coupling terms in the 12×12 hydrodynamic coefficient matrix). In this paper, an exact time-domain simulation method including all the 12×12 hydrodynamic coefficients in a hull-line combined matrix is developed and called the CMM. With this exact solution available, the performance of the two approximation methods can be tested for various environmental conditions.

Our numerical examples for two different environmental conditions (co-linear wind, wave, and current in the head direction) illustrate that there may be large discrepancy between the CMM and the approximation methods. The SMM is better than the NHI but may still significantly over-predict or under-predict the actual relative motions, hawser and mooring tension, and fender forces. This means that even the cross-coupling (off-diagonal block) terms of the full hydrodynamic coefficient matrix play an important role in the case of side-by-side offloading operation. Therefore, such approximation methods should be used with care.

The present study was carried out in the context of potential theory, which is known to produce reasonable motion results except roll. The pumping mode in the gap caused negative added mass and large motions. Viscous effects and nonlinearity may further reduce the roll motions and the pumping mode. The discrepancy between the exact (CMM) and other approximation methods (SMM, NHI) may even be greater in non-parallel or beam-sea conditions. Those will be the subjects of future study.

Acknowledgements

This research is financially supported by MMS (Minerals Management Service) and OTRC (Offshore Technology Research Center).

References

- [1] Arcandra T. Hull/mooring/riser coupled dynamic analysis of a deepwater floating platform with polyester lines. Ph.D. dissertation. College Station (TX): Civil Engineering Department, Texas A&M University; 2001.
- [2] Arcandra T, Prahoro N, Kim MH. Effect of line dynamics and hull viscous drag on the motion of turret-moored FPSO. In: OMAE special conference on FPSO integrity. 2004.
- [3] Buchner B, Dijk A, Wilde J. Numerical multiple-body simulations of side-by-side mooring to an FPSO. In: Proc. 11th int. offshore and polar eng. conference, ISOPE, vol. 1. 2001. p. 343–53.
- [4] Choi YR, Hong SY. An analysis of hydrodynamic interaction of floating multi-body using higher-order boundary element method. Proc. 12th int. offshore and polar eng. conference, ISOPE, vol. 1. 2002. p. 303–8.
- [5] Fang MC, Kim CH. Hydrodynamically coupled motions of two ship advancing in oblique waves. *Journal of Ship Research* 1986;30(3): 159–71.
- [6] Garrett DL. Dynamic analysis of slender rods. *Journal Energy Resources Technology* 1982;104:302–7.
- [7] Hong SY, Kim JH, Cho SK, Choi YR, Kim YS. Numerical and experimental study on hydrodynamic interaction of side-by-side moored multiple vessels. In: Proc. of deep water mooring system. ASCE; 2003. p. 198–215.
- [8] Huijsmans RHM, Pinkster JA, de Wilde JJ. Diffraction and radiation of waves around side-by-side moored vessels. In: Proc. 11th int. offshore and polar eng. conference, ISOPE, vol. 1. 2001. p. 406–12.
- [9] Kim MH, Arcandra T, Kim YB. Validability of spar motion analysis against various design methodologies/parameters. In: Proc. 20th offshore mechanics and arctic eng. conference. OMAE01-OFT1063 [CD-ROM] 2001.
- [10] Kim MH, Arcandra T, Kim YB. Validability of TLP motion analysis against various design methodologies/parameters. In: Proc. 11th int. offshore and polar eng. conference, ISOPE, vol. 3. 2001. p. 465–73.
- [11] Kim MH, Kim YB. Hull-mooring-riser coupled dynamic analysis of a tanker-based turret-moored FPSO in deep water. In: Proc. 12th int. offshore and polar eng. conference, ISOPE02. 2002.
- [12] Kim MH, Koo BJ, Mercier RM, Ward EG. Vessel-mooring-riser coupled dynamic analysis of a turret-moored FPSO compared with OTRC experiment. *Journal of Ocean Engineering* 2005;32:1780–802.
- [13] Kim YB. Dynamic analysis of multiple-body floating platforms coupled with mooring lines and risers. Ph.D. dissertation. College Station (TX): Civil Engineering Department, Texas A&M University; 2003.
- [14] Kodan N. The motion of adjacent floating structure in oblique waves. Proc. 3rd offshore mechanics and Arctic eng. conference, vol. 1. 1984. p. 206–13.
- [15] Koo BJ, Kim MH, Randall RE. The effect of nonlinear multi-contact coupling with gap between risers and guide frames on global spar motion analysis. *Journal of Ocean Engineering* 2004;31(11–12):1469–502.
- [16] Koo BJ, Kim MH. Motion analysis of two floating platform with mooring and hawser lines in tandem moored operation by combined matrix method and separated matrix. *Journal of Ocean Engineering and Technology* 2005;19:1–15.
- [17] Lee DH. Nonlinear stability analysis and motion control of tandem moored tankers. Ph.D. dissertation. Seoul: Naval Architecture and Ocean Engineering, Seoul National University; 2002.
- [18] Lee CH. WAMIT theory manual. MA: Department of Ocean Engineering. MIT; 1999.
- [19] Lee DH, Choi HS. A dynamic analysis of FPSO-shuttle tanker system. In: Proc. 10th int. offshore and polar eng. conference, ISOPE, vol. 1. 2000. p. 302–7.
- [20] Loken AE. Hydrodynamic interaction between several floating bodies of arbitrary form in waves. Proc. of int'l symposium on hydrodynamics in ocean engineering, NIT, vol. 2. 1981. p. 745–79.
- [21] Ma W, Lee MY, Zou J, Huang EW. Deepwater nonlinear coupled analysis tool. In: Offshore Technology Conference. 2000.
- [22] OCIMF. Prediction of wind and current loads on VLCCs. 2nd ed. London (England): Witherby & Co. Ltd; 1994.
- [23] Ohkush M. Ship motions in vicinity of a structure. In: Proc. of int'l conf. on behavior of offshore structure, NIT, vol. 1. 1974. p. 284–306.
- [24] Paulling JR, Webster WC. A consistent large-amplitude analysis of the coupled response of a TLP and tendon system. In: Proceeding of the 5th offshore mechanics and arctic engineering symposium, vol. 3. 1986. p. 126–33.
- [25] Sphaier SH, Fernandes AC, Correa SH. Maneuvering model for the FPSO horizontal plane behavior. In: Proc. 10th int. offshore and polar eng. conference, ISOPE, vol. 1. 2000. p. 337–44.
- [26] Van Oortmerssen G. Hydrodynamic interaction between two structures of floating in waves. In: Proc. Boss '79. 2nd int'l conf. on behavior of offshore structure. 1979. p. 339–56.
- [27] Wichers JEW, Voogt HJ, Roelofs HW, Driessen PCM. DeepStar-CTR 4401- benchmark model test. Technical rep. no. 16417-1-OB, MARIN, Wageningen, Netherlands; 2001.
- [28] Wichers JEW, Develin PV. Effect of coupling of mooring lines and risers on the design values for a turret moored FPSO in deep water of the gulf of Mexico. In: Proc. 11th int. offshore and polar eng. conference, ISOPE, vol. 3. 2001 p. 480–7.
- [29] Wichers JEW. A simulation model for a single point moored tanker. Ph.D. dissertation. Delft (The Netherlands): Delft University of Technology; 1988.